TBK1-mTOR Signaling Attenuates Obesity-Linked Hyperglycemia and Insulin Resistance

Cagri Bodur,[1] Dubek Kazyken,[1] Kezhen Huang,[1] Aaron Seth Tooley,[1] Kae Won Cho,[2] Tammy M. Barnes,[3] Carey N. Lumeng,[2] Martin G. Myers Jr.,[3] and Diane C. Fingar[1]

Diabetes 2022;71:2297–2312 | https://doi.org/10.2337/db22-0256

The innate immune kinase TBK1 (TANK-binding kinase 1) responds to microbial-derived signals to initiate responses against viral and bacterial pathogens. More recent work implicates TBK1 in metabolism and tumorigenesis. The kinase mTOR (mechanistic target of rapamycin) integrates diverse environmental cues to control fundamental cellular processes. Our prior work demonstrated in cells that TBK1 phosphorylates mTOR (on S2159) to increase mTORC1 and mTORC2 catalytic activity and signaling. Here we investigate a role for TBK1-mTOR signaling in control of glucose metabolism in vivo. We find that mice with diet-induced obesity (DIO) but not lean mice bearing a whole-body "TBK1-resistant" *Mtor* S2159A knock-in allele (*Mtor*$^{A/A}$) display exacerbated hyperglycemia and systemic insulin resistance with no change in energy balance. Mechanistically, *Mtor* S2159A knock-in in DIO mice reduces mTORC1 and mTORC2 signaling in response to insulin and innate immune agonists, reduces anti-inflammatory gene expression in adipose tissue, and blunts anti-inflammatory macrophage M2 polarization, phenotypes shared by mice with tissue-specific inactivation of TBK1 or mTOR complexes. Tissues from DIO mice display elevated TBK1 activity and mTOR S2159 phosphorylation relative to lean mice. We propose a model whereby obesity-associated signals increase TBK1 activity and mTOR phosphorylation, which boost mTORC1 and mTORC2 signaling in parallel to the insulin pathway, thereby attenuating insulin resistance to improve glycemic control during diet-induced obesity.

TBK1 (TANK-binding kinase 1), a noncanonical IKK-related innate immune kinase, responds to microbial-derived signals to initiate host defense responses against viral and bacterial pathogens (1,2). More recent work implicates TBK1 in energy storage, improved glycemic control, suppression of proinflammatory responses, and tumorigenesis, revealing TBK1 as a multifunctional kinase (3–10). The conserved kinase mTOR (mechanistic target of rapamycin) functions as a metabolic rheostat by integrating multiple environmental cues to control fundamental cellular functions important for diverse physiological processes (11–14). mTOR mediates its myriad cellular functions as the catalytic core of two distinct, multisubunit complexes, mTORC1 (defined by the partner Raptor) and mTORC2 (defined by the partner Rictor). Aberrant mTOR complex signaling—either too high or too low—thus contributes to many pathological conditions including type 2 diabetes, cancer, and immunological disorders (13,15). Despite the physiological importance of TBK1 and mTOR complexes, our mechanistic understanding of how these kinases control diverse processes remains incomplete, particularly in in vivo settings. In our prior work we identified TBK1 as a previously unknown upstream activator of mTORC1 and mTORC2 in intact cells: we found that TBK1 interacts with and phosphorylates mTOR (on S2159) to increase mTORC1 and mTORC2 catalytic activity and downstream signaling (16,17). Studies from other groups agree that TBK1 positively regulates mTOR complexes (18,19).

Insulin and related IGFs activate both mTORC1 and mTORC2 in a PI3K-dependent manner (14,20,21), although regulation of mTORC1 remains better defined than that of mTORC2 (14,21). Insulin/PI3K signals through Akt (phosphorylation on T308 [P-T308]), TSC, and Rheb to activate

[1]Department of Cell and Developmental Biology, University of Michigan Medical School, Ann Arbor, MI
[2]Department of Pediatrics and Communicable Diseases, University of Michigan Medical School, Ann Arbor, MI
[3]Department of Internal Medicine, Division of Metabolism, Endocrinology, and Diabetes, University of Michigan Medical School, Ann Arbor, MI
Corresponding author: Diane C. Fingar, dfingar@umich.edu

Received 14 March 2022 and accepted 15 August 2022

This article contains supplementary material online at https://doi.org/10.2337/figshare.20496951.

mTORC1 on lysosomal membranes after amino acid–induced recruitment of mTORC1 to lysosomes (12–14). mTORC1 drives anabolic (e.g., protein, lipid, and nucleotide synthesis) and suppresses catabolic (e.g., autophagy) cellular metabolism through phosphorylation of downstream targets such as S6K1 (T389). In turn, mTORC1 promotes cell growth and proliferation (13,14). On activation by insulin/PI3K, mTORC2 phosphorylates Akt (S473), which controls distinct metabolic processes in parallel to Akt/mTORC1 and promotes cell survival (14,20–23). mTORC1 and mTORC2 play complex roles in glucose and lipid metabolism in vivo, particularly during diet-induced obesity (15). Adipocyte-specific knockout of *Raptor* indicates that mTORC1 promotes adipose tissue expansion and suppresses adipose tissue inflammation (15,24–26). Adipocyte- or hepatocyte-specific knockout of *Rictor* indicates that mTORC2/Akt (P-S473) promotes glucose uptake and lipogenesis in adipose and liver tissues and suppresses hepatic gluconeogenic gene expression and glucose production by the liver in response to insulin (27,28).

TBK1 and its tissue-restricted ortholog IKKε (Iκβ kinase ε) mediate innate immune responses by inducing transcription of type I interferons (e.g., IFNα/β) in macrophages and related phagocytic cells (1,2). Microbial-derived signals such as viral double-stranded RNA (dsRNA) or bacterial lipopolysaccharide (LPS) activate the pathogen recognition receptors toll-like receptor (TLR)3 or TLR4, respectively, leading to activation of TBK1 and IKKε on phosphorylation of their essential activation loop sites (S172), possibly by an induced dimerization and autophosphorylation mechanism or by an unknown upstream kinase (29,30). When activated, TBK1/IKKε phosphorylate the transcription factors IRF3 and 7, inducing their nuclear translocation and the consequent induction of type I IFNs (1,2). Our prior work showed that TBK1 signaling to mTORC1 also facilitates the nuclear translocation of IRF3 and the transcriptional induction of IFNβ (16). Type I IFNs in turn induce interferon-stimulated genes, which not only mediate antimicrobial responses but also promote anti-inflammatory responses that resolve acute inflammation and limit tissue damage (1,2,31).

More recent work implicates TBK1 in energy storage and glycemic control, particularly during diet-induced obesity, a pathologic state linked to myriad metabolic disorders including insulin resistance and chronic inflammation (3–7,32). Treatment of mice with diet-induced obesity (DIO) with amlexanox (a pharmacological inhibitor of TBK1 and IKKε) reduces body weight and adiposity through increased energy expenditure (3). These mice also display improved insulin sensitivity and glycemic control, likely due in part to decreased obesity (3). Clinically, amlexanox also reduces body weight and improves glycemic control in obese patients (4), revealing TBK1 and IKKε as potential new therapeutic targets for the treatment of obesity. Similar to system-wide inhibition of TBK1/IKKε with amlexanox (3), global reduction of TBK1 kinase activity in DIO mice due to expression of truncated TBK1 alleles ($Tbk1^{\Delta/\Delta}$) (6) reduces body weight and adiposity with consequent improvements in glycemic control, insulin sensitivity, and inflammatory state (6). Interestingly and unexpectedly, despite a modest reduction in adiposity with no significant change in body weight, adipocyte-specific *Tbk1* knockout mice display exacerbated systemic insulin resistance and adipose tissue inflammation during diet-induced obesity (5). Taken together, these findings suggest complex roles for TBK1 in metabolic control: TBK1 inactivation exerts beneficial (reduced adiposity) and detrimental (increased insulin resistance and inflammation) metabolic effects in the context of diet-induced obesity (3,5,7). The downstream effectors used by TBK1 to control energy balance, insulin sensitivity, and inflammatory state remain poorly defined, however.

Tissue-specific knockout mouse models reveal overlapping roles for TBK1 and mTOR complexes in control of systemic insulin sensitivity and glucose homeostasis (5,15,24,27,28,33). Strikingly, adipocyte-specific knockout of *Tbk1*, *Mtor*, *Raptor* (mTORC1 deficient), or *Rictor* (mTORC2 deficient) (using adiponectin-Cre) exacerbates systemic insulin resistance during diet-induced obesity, thus impairing glycemic control (5,24,25,28,33). We therefore tested the hypothesis that TBK1 and mTOR work together in the same pathway to control glucose metabolism in vivo. To do so, we studied a "TBK1-resistant" whole-body (i.e., global) *Mtor* knock-in mouse model bearing a nonphosphorylatable *Mtor* S2159A allele ($Mtor^{A/A}$), generated in our prior work (16). We report here that *Mtor* S2159A knock-in exacerbates hyperglycemia and systemic insulin resistance during DIO. Mechanistically, *Mtor* S2159A knock-in in DIO mice reduces mTORC1 and mTORC2 signaling in response to insulin, reduces anti-inflammatory gene expression in adipose tissue, and blunts anti-inflammatory macrophage M2 polarization. Interestingly, reduced TBK1-mTOR signaling exacerbates insulin resistance in obese but not lean male mice and in DIO male but not female mice, revealing context-dependent function for TBK1-mTOR signaling. As we find elevated TBK1 activity and mTOR S2159 phosphorylation in tissues from DIO mice relative to lean mice, we propose a model whereby obesity-associated signals increase TBK1 activity and mTOR phosphorylation in parallel to the insulin pathway, which boost mTORC1 and mTORC2 signaling to improve glycemic control.

RESEARCH DESIGN AND METHODS

Materials

General chemicals were from Thermo Fisher Scientific or Sigma-Aldrich. NP40 and Brij35 detergents were from Pierce; Pierce Protease Inhibitor Mini Tablets, EDTA-Free, were from Thermo Fisher Scientific (no. A32955), PhosSTOP phosphatase inhibitor cocktail tablets were from Roche (no. 04906845001), 4× Laemmli Sample Buffer was from Bio-Rad Laboratories (no. 1610747), Protein A Sepharose Fast Flow beads were from GE Healthcare, Immobilon-P PVDF Membrane (0.45 μmol/L) was from Millipore, and reagents for enhanced chemiluminescence were from either

Alkali Scientific (BrightStar) or Advansta (WesternBright Sirius horseradish peroxidase substrate).

Generation of *Mtor*$^{A/A}$ Mice

Mtor$^{A/A}$ mice were generated with CRISPR/Cas9 genome editing technology and genotyped as previously described (16). Mice were housed in a specific pathogen-free facility with a 12-h light/12-h dark cycle and given free access to food and water, except for brief fasts prior to assays of glycemic control, as noted below. All animal use was approved by the Institutional Animal Care and Use Committee at the University of Michigan.

Metabolic Phenotyping of Mtor$^{+/+}$ *and* Mtor$^{A/A}$ *Mice*

Mice were fed either a normal chow diet (NCD) (no. 5001; Purina LabDiet) or a high-fat diet (HFD) (no. D12492, 60% calories from fat; Research Diets) beginning at 4 weeks old. Weekly body weight and biweekly ad libitum fed blood glucose levels were monitored. For insulin tolerance tests (ITT), mice were fasted for 5 h and then insulin (Humulin R; Eli Lilly) was injected (1.0 unit/kg body wt i.p. for NCD-fed mice or 1.3 units/kg body wt i.p. for HFD-fed mice). Blood glucose was measured at time t = 0, 15, 30, 60, and 120 min with a handheld glucometer (OneTouch Ultra 2; LifeScan). For glucose tolerance tests (GTT), mice were fasted for 20 h and then glucose (2 g/kg body wt i.p., Dextrose; Hospira) was injected into mice fed an NCD or HFD. Blood glucose was measured as described above for ITT. Blood plasma samples were collected in mice fed an NCD (at 16 weeks old) and in mice fed an HFD for 8, 14, and 20 weeks (at 12, 18, and 24 weeks old). Insulin levels were measured by commercial ELISA (no. 90080; Crystal Chem). Body composition of DIO mice (after 20 weeks of HFD feeding) was measured with a nuclear magnetic resonance–based analyzer (minispec LF90ll; Bruker Optics) at the University of Michigan (UM) Animal Phenotyping Core.

Administration of Polyinosinic-Polycytidylic Acid, LPS, and Insulin In Vivo

Lean mice fed an NCD ad libitum (8- to 14-week-old males) were injected intraperitoneally with PBS or 0.9% saline (as indicated in the figure legend), polyinosinic-polycytidylic acid (poly[I:C]) (10 mg/kg body wt, no. P1530; Sigma-Aldrich), or LPS (1 mg/kg body wt, no. tlrl-3pelps; InvivoGen) for 2 h. For experiments with insulin, lean mice fed an NCD (8–14 weeks old) or DIO mice fed an HFD for 20 weeks (24-week-old males and females) were injected intraperitoneally with 0.9% saline or insulin for 30 min after a 5-h fast (1.0 unit/kg body wt for NCD-fed mice and 1.3 units/kg body wt for HFD-fed mice). Mice were euthanized postinjection, and tissues were dissected out and flash-frozen for analysis by Western blot.

Cell Lysis, Tissue Homogenization, Immunoprecipitation, and Immunoblotting

For lysing bone marrow–derived macrophage (BMDMs) and mouse embryonic fibroblasts (MEFs) in culture, cells were washed twice with ice-cold PBS, pH 7.4, and scraped into ice-cold lysis buffer A (10 mmol/L KPO_4, pH 7.2; 1 mmol/L EDTA; 5 mmol/L EGTA; 10 mmol/L $MgCl_2$; 50 mmol/L β-glycerophosphate) containing NP-40 (0.5%) and Brij35 (0.1%) as well as protease and phosphatase inhibitors. To lyse gonadal (gWAT) and inguinal (iWAT) white adipose tissues, samples were homogenized in 1 mL ice-cold TNE buffer (50 mmol/L Tris, 150 mmol/L NaCl, 1 mmol/L EDTA, pH 8.0) with protease and phosphatase inhibitors with a TissueRuptor (QIAGEN). Homogenates were centrifuged at 5,000 rpm for 5 min at 4°C, and Triton X-100 was added (2% final) to the aqueous phase for lysis. To lyse liver (~100 mg), skeletal muscle (soleus), and spleen tissues, we homogenized and lysed samples in ice-cold 1 mL radioimmunoprecipitation assay buffer with protease and phosphatase inhibitors. Lysates were centrifuged at 13,200 rpm for 15 min at 4°C, and supernatant was collected. Protein levels were normalized across samples with DC protein assay (no. 5000111; Bio-Rad Laboratories). For mTOR immunoprecipitation from spleen or liver lysates, a custom anti-mTOR peptide antibody (amino acids 221–237, rat) was used (34). mTOR antibody was added to lysates for 2 h at 4°C, followed by incubation with Protein A Sepharose beads for 1 h. Beads were washed three times in lysis buffer and resuspended in 1× Laemmli sample buffer. Immunoblotting was performed as previously described (16). For monitoring of mTOR S2159 phosphorylation, a custom anti–mTOR-P-S2159 peptide antibody was made in collaboration with Millipore, as previously described (16). All other antibodies were from Cell Signaling Technology: P-S6K1 T389 (no. 9205), S6K1 (no. 9202), P-Akt S473 (no. 4060), Akt (no. 9272), P-TBK1 S172 (no. 5483), TBK1 (no. 3504), mTOR (no. 2972), IKKε (no. 3416), and β-actin (no. 4970).

Isolation and Treatment of Primary BMDMs

Bone marrow was harvested by flushing femora and tibiae from mice at 8–14 weeks of age with cold PBS with a 30 G needle (BD) under sterile conditions. Bone marrow cells were suspended in minimum essential medium with L-glutamine supplemented with 10% heat-inactivated FBS, 50 units/mL penicillin, 50 μg/mL streptomycin, and 20 ng/mL M-CSF (no. 416-ML; R&D Systems) and plated into sixwell tissue culture plates. Cells were incubated at 37°C in a humidified atmosphere with 5% CO_2, and medium was replaced every other day until day 5, when the experiments were done around 80% confluency. BMDMs were pretreated without or with Torin1 (100 nmol/L) (shared by Dr. D. Sabatini, MIT, and the Whitehead Institute, Cambridge, MA), Ku-0063794 (1 μmol/L, no. 3725; Tocris), or amlexanox (100 μmol/L, 485710; Tocris), and then stimulated without or with poly(I:C) (30 μg/mL). To induce M2 polarization, we treated BMDMs with IL-4 (10 ng/mL, no. 214-14; Peprotech) for 24 h or with PBS (negative control).

Histology

Liver and gWAT samples <10 mm in length and 4 mm in thickness were dissected out and fixed in 25 mL 10% neutral buffered formalin for 72 h at room temperature. Samples were next dehydrated in 20% sucrose (in PBS) overnight at 4°C. Tissue samples were embedded in optimal cutting temperature (OCT) compound and frozen on dry ice before submission to the UM Animal Phenotyping Core for histological (oil red O and hematoxylin-eosin [H-E]) and immunohistochemical (F4/80) staining.

RNA Isolation and Quantitative RT-PCR

Total RNA was isolated from BMDMs with an RNeasy Plus Mini Kit (no. 74134; QIAGEN) and from gWAT (~100 mg) and liver (~30 mg) with use of QIAzol Lysis Reagent (no. 79306; QIAGEN) according to the manufacturer's protocols. Reverse transcription was done with a High-Capacity RNA-to-cDNA Kit (no. 4387406; Thermo Fisher Scientific). Quantitative (q)PCR was performed with a StepOnePlus Real-Time PCR machine (Applied Biosystems) using Radiant Probe master mix (no. QP8001; Alkali Scientific) for TaqMan gene assays and Radiant Green master mix (no. QS2001; Alkali Scientific) for SYBR Green assays. Relative quantification was performed with the ΔΔCT method. Assay identifiers for the predesigned TaqMan gene expression assays (4331182; Thermo Fisher Scientific) were as follows: Mm00439552-s1 (*Ifnb1*), Mm00802529_m1 (F4/80), Mm00441242_m1 (*Ccl2*), Mm01302427_m1 (*Ccl5*), Mm00475988_m1 (*Arg1*), Mm00546125_g1 (*Mgl1*), Mm00460844_m1 (*Mgl2*), Mm01288386_m1 (*Il10*), Mm00445109_m1 (*Fizz1*), Mm00657889_m1 (*Ym1*), Mm00498701_m1 (*Cd11c*), Mm00446190_m1 (*Il6*), Mm00434228_m1 (*Il1b*), Mm00443258_m1 (*Tnfa*), Mm00440502_m1 (*Nos2*), Mm00839363_m1 (*G6pase*), Mm01247058_m1 (*Pepck*), Mm00490181_m1 (*Fbp1*), Mm01304257_m1 (*Acc*), Mm01302282_m1 (*Acl*), and Mm00662319_m1 (*Fas*). GAPDH (Mm99999915-g1) was used as an endogenous control for normalization in TaqMan qPCRs. *Chrebpb* forward (5′-TCTGCAGATCGCGTGGAG-3′) and reverse (5′-CTTGTCCCGGCATAGCAAC-3′) primers were purchased from IDT. A predesigned *Gapdh* qPCR assay (Mm.PT.39a.1; IDT) was used as endogenous control for *Chrebpb* analysis.

Isolation and Immortalization of MEFs

Male and female heterozygous $Mtor^{+/A}$ mice were mated, and primary MEFs from plugged females were isolated on day 13.5 of pregnancy, generally as previously described (35,36) (see also 17). MEFs were genotyped using dissected head tissue as previously described (16). Primary $Mtor^{+/+}$ and $Mtor^{A/A}$ MEFs were then immortalized spontaneously by serial passaging as previously described (17). Immortalized MEFs at ~80–90% confluency were serum deprived (20 h), pretreated without or with Torin1 (100 nmol/L) (30 min), and stimulated without or with insulin (100 nmol/L, no. 12585; Invitrogen) (5 or 30 min) or LPS (1 μg/mL, no. tlrl-3pelps; InvivoGen) (5–120 min).

Quantification and Statistical Analysis

Bar graphs and box and whisker plots were generated with GraphPad Prism 9. Line graphs were generated with Microsoft Excel. Line and bar graphs represent means ± SEM; box-and-whisker plots represent mean (the + symbol indicates the mean value), median, and quartiles. Statistical analyses were performed with Excel or GraphPad Prism 9. Statistical significance between two mean values was tested with two-tailed unpaired Student *t* test with an assumption of equal variances. Statistical significance of blood glucose over time in wild-type versus $Mtor^{A/A}$ mice was tested with use of mixed-effects analysis of multiple comparisons followed by Bonferroni post hoc tests. This model was used rather than two-way ANOVA with repetition to better handle missing data points (i.e., a limited number of mice lacked a biweekly blood glucose measurement). Statistical significance of plasma insulin levels and insulin tolerance (ITTs) over time in wild-type versus $Mtor^{A/A}$ mice was tested with two-factor ANOVA with repetition followed by Bonferroni post hoc tests. Asterisks are used to indicate statistical significance: $*P < 0.05$; $**P < 0.01$; $***P < 0.001$. Western blot images were prepared for publication with Adobe Photoshop. Only the parameters levels, brightness, and contrast were used to fine-tune exposure time and band sharpness. Importantly, these parameters were adjusted equivalently across the entire blot, and the final image shown reflects the raw image. In certain panels, thin dotted lines indicate excision of an irrelevant lane(s) from a Western blot. Western blot signals were quantitated with Fiji (ImageJ) to measure integrated densities of protein bands. The ratios of phosphorylated proteins over cognate total protein were calculated and normalized as indicated in the figure legends.

Data and Resource Availability

All data generated or analyzed during this study are included in the published article and Supplementary Material. Resources generated in the current study are available from the corresponding author on reasonable request.

RESULTS

Primary Macrophages and Tissues From $Mtor^{A/A}$ Mice Display Reduced mTORC1 and mTORC2 Signaling in Response to Innate Immune Agonists

As demonstrated in our prior work (16,17), we confirmed that TBK1-mediated mTOR S2159 phosphorylation promotes mTORC1 and mTORC2 signaling in primary macrophages. BMDMs from $Mtor^{A/A}$ mice displayed reduced mTORC1 (S6K1 P-T389) and mTORC2 (Akt P-S473) signaling in response to poly(I:C), a viral dsRNA mimetic that activates TLR3 (Fig. 1*A*). Importantly, poly(I:C) activated TBK1 similarly in $Mtor^{+/+}$ and $Mtor^{A/A}$ BMDMs, as monitored through phosphorylation of TBK1 on its essential activation loop site (S172) (Fig. 1*A*), and BMDMs from $Mtor^{A/A}$ mice lacked mTOR S2159 phosphorylation (Fig. 1*B*). As expected, the mTOR inhibitor Torin1 suppressed

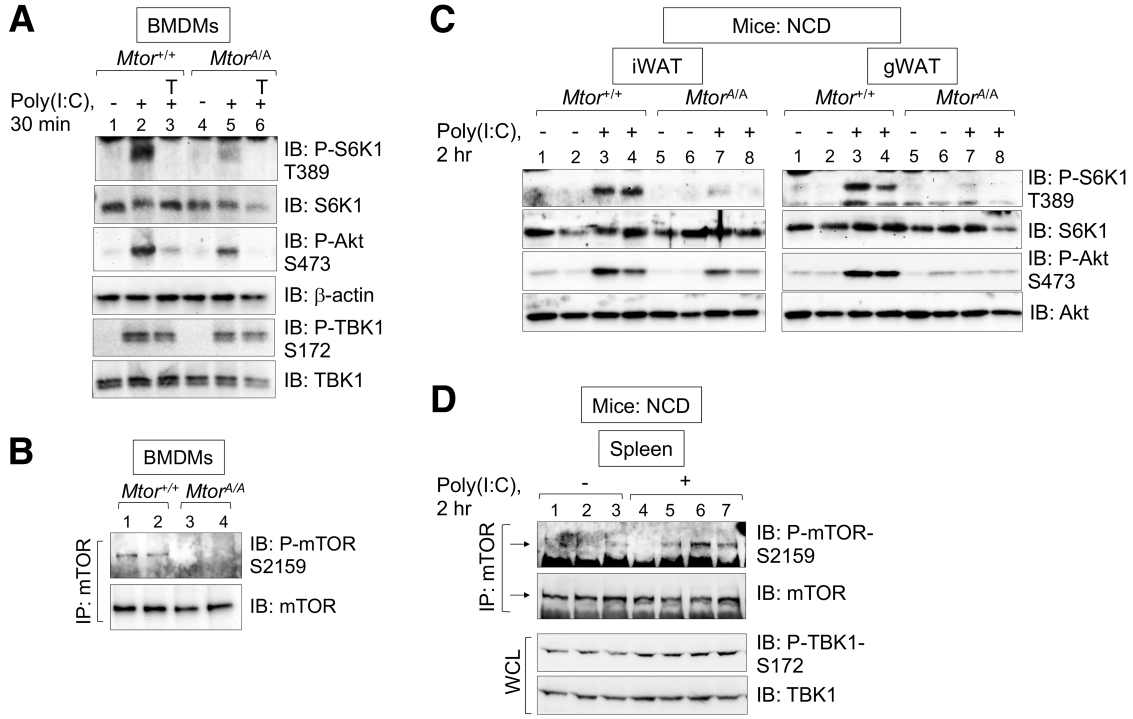

Figure 1—Primary macrophages and tissues from *Mtor*$^{A/A}$ mice display reduced mTORC1 and mTORC2 signaling in response to innate immune agonists. *A*: Reduced mTORC1/2 signaling in BMDMs from *Mtor*$^{A/A}$ mice in response to poly(I:C). BMDMs from *Mtor*$^{+/+}$ and *Mtor*$^{A/A}$ mice were pretreated in culture with the mTOR inhibitor Torin1 (100 nmol/L, 30 min) and stimulated without (−) or with (+) poly(I:C) (30 μg/mL, 30 min). Whole cell lysates were immunoblotted (IB) as indicated. *B*: mTOR P-S2159 in untreated BMDMs from *Mtor*$^{A/A}$ mice. mTOR was immunoprecipitated (IP) in duplicate from *Mtor*$^{+/+}$ and *Mtor*$^{A/A}$ BMDM lysates and immunoblotted as indicated. *C*: Reduced mTORC1/2 signaling in WAT from lean *Mtor*$^{A/A}$ mice in response to poly(I:C) in vivo. *Mtor*$^{+/+}$ and *Mtor*$^{A/A}$ mice (8–14 weeks old) were injected with saline or poly(I:C) (10 mg/kg body wt, 2 h) in duplicate following a 5-h fast. Tissue lysates were immunoblotted as indicated (four mice per genotype). Each lane represents an individual mouse. *D*: mTOR P-S2159 in vivo in lean *Mtor*$^{+/+}$ mice in response to poly(I:C). Lean mice (C57BL/6) (8 weeks old) were injected intraperitoneally with PBS or poly(I:C) (10 mg/kg body wt) (2 h) in triplicate. mTOR was immunoprecipitated from spleen tissue lysates, and IPs and whole cell lysates (WCL) were immunoblotted as indicated. Each lane represents an individual mouse. hr, hours.

activation of mTORC1 and mTORC2 signaling by poly(I:C) in wild-type BMDMs (Fig. 1*A*). These data confirm that TLR3-mediated activation of mTORC1 and mTORC2 signaling in BMDMs requires mTOR S2159 phosphorylation and activity.

We next administered poly(I:C) to mice by intraperitoneal injection. In iWAT (subcutaneous fat) and gWAT (visceral fat), poly(I:C) increased mTORC1 and mTORC2 signaling in *Mtor*$^{+/+}$ but not *Mtor*$^{A/A}$ tissue (Fig. 1*C*), consistent with our prior results in spleen tissue (17). While the mTOR P-S2159 signal was too weak to assess reliably in adipose tissues, we confirmed that poly(I:C) increases mTOR P-S2159 in spleen tissue from wild-type mice (Fig. 1*D*). Activation of TLR4 with LPS administration in vivo also increased mTOR P-S2159 in spleen tissue from wild-type mice (Supplementary Fig. 1*A*) and increased mTORC1 and mTORC2 signaling in spleen tissue from wild-type but not *Mtor*$^{A/A}$ mice (Supplementary Fig. 1*B*). These results indicate that activation of TLR3 or TLR4 in vivo increases mTOR P-S2159 and promotes mTORC1/2 signaling in a manner dependent on mTOR P-S2159.

Unaltered Systemic Insulin Sensitivity and Insulin-Responsive mTORC1/2 Signaling in Lean *Mtor*$^{A/A}$ Mice

We next measured several metabolic parameters longitudinally in lean *Mtor*$^{+/+}$ and *Mtor*$^{A/A}$ mice fed an NCD. Weekly body weight and biweekly ad libitum feeding blood glucose levels did not differ between the two genotypes (Fig. 2*A* and *B*). Systemic insulin sensitivity and glucose tolerance were similar in *Mtor*$^{+/+}$ and *Mtor*$^{A/A}$ mice, as measured by ITT (Fig. 2*C*) and GTT tests (Fig. 2*D*). We next analyzed mTORC1 and mTORC2 signaling in response to insulin in several target tissues. Intraperitoneal insulin injection (30 min) activated mTORC1 (S6K1 P-T389) and mTORC2 (Akt P-S473) signaling similarly in adipose tissues (iWAT and gWAT), liver, and skeletal muscle (soleus) from *Mtor*$^{+/+}$ and *Mtor*$^{A/A}$ mice (Fig. 2*E*). Together, these results demonstrate that mTOR P-S2159 is dispensable in lean mice for whole-body energy balance, glycemic control, insulin sensitivity, and mTORC1/2 signaling. Consistent with the in vivo results above, insulin-stimulated activation of mTORC1/2 signaling was intact in primary MEFs isolated from *Mtor*$^{A/A}$

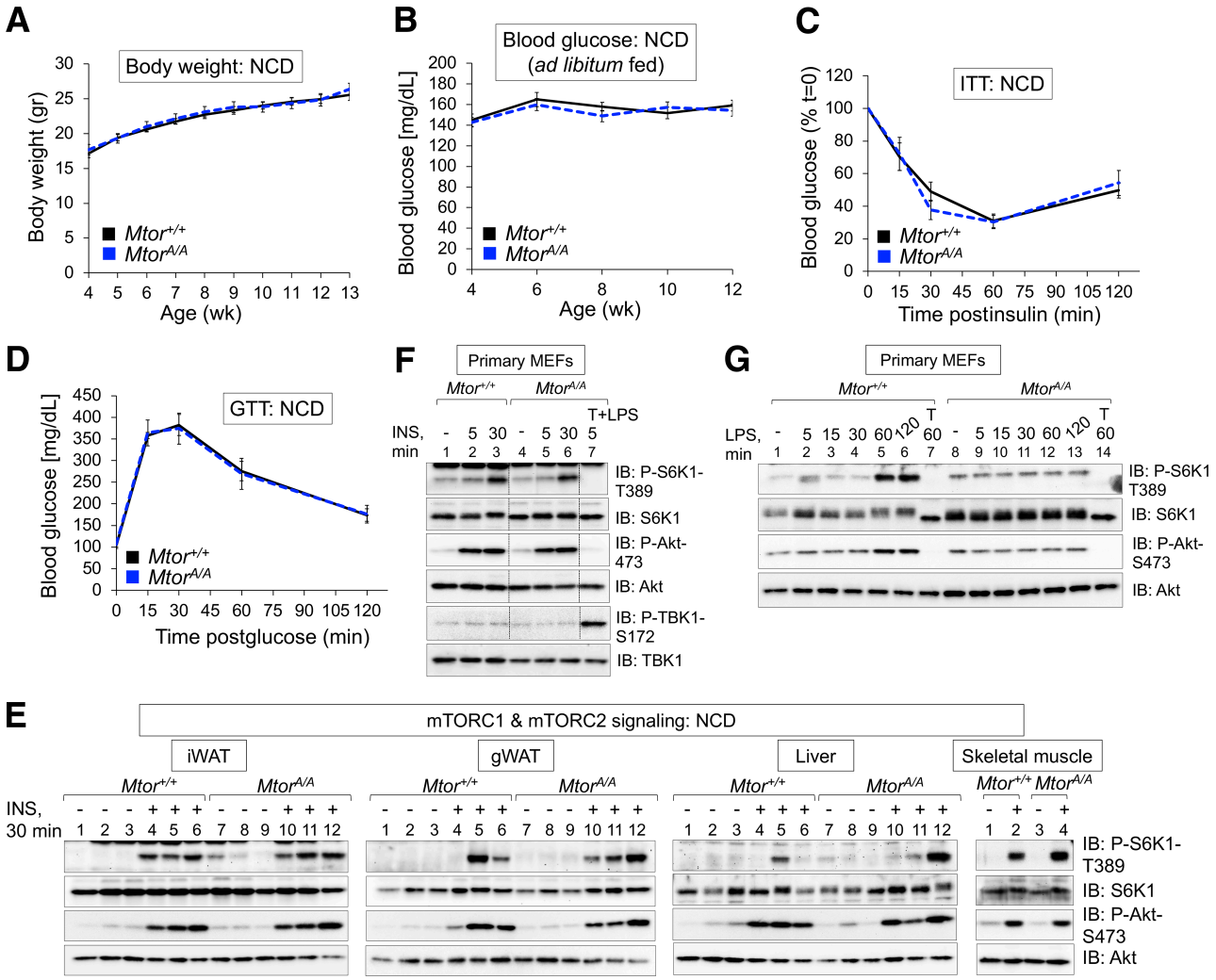

Figure 2—Unaltered systemic insulin sensitivity and insulin-responsive mTORC1/2 signaling in lean *Mtor*$^{A/A}$ mice. *Mtor*$^{+/+}$ and *Mtor*$^{A/A}$ male mice were fed an NCD for 16 weeks. The following metabolic parameters were measured. *A*: Weekly body weight. n = 12 *Mtor*$^{+/+}$, 14 *Mtor*$^{A/A}$. *B*: Bi-weekly blood glucose. n= 12 *Mtor*$^{+/+}$, 14 *Mtor*$^{A/A}$. *C*: Systemic insulin sensitivity was measured by ITT at 15 weeks of age. Blood glucose was measured before and after injection of insulin (1.0 units/kg body wt i.p.). n = 10 *Mtor*$^{+/+}$, 12 *Mtor*$^{A/A}$. *D*: Systemic glucose tolerance was measured by GTT at 14 weeks of age. Blood glucose was measured before and after injection of glucose (2 g/kg body wt i.p.). n = 10 *Mtor*$^{+/+}$, 12 *Mtor*$^{A/A}$. *E*: Intact insulin-responsive mTORC1/2 signaling in tissues from *Mtor*$^{A/A}$ mice. *Mtor*$^{+/+}$ and *Mtor*$^{A/A}$ mice were injected without (−) or with (+) insulin (1.0 units/kg body wt, 30 min.) following a 5-h fast. iWAT, gWAT, liver, and skeletal muscle lysates were immunoblotted as indicated. Each lane represents an individual mouse. *F*: Intact insulin-responsive mTORC1/2 signaling in primary MEFs from *Mtor*$^{A/A}$ mice. Primary MEFs were serum starved (20 h), pretreated with the mTOR inhibitor Torin1 (100 nmol/L, 30 min), and stimulated without (−) or with (+) insulin (100 nmol/L), as indicated. Whole cell lysates were immunoblotted as indicated. In lane 7 (positive control for TBK1 activation), MEFs were serum starved overnight in the presence of LPS (1 μg/mL), treated with Torin1 as described above, and stimulated with insulin for 5 min. *G*: Impaired LPS-responsive mTORC1/2 signaling in primary MEFs from *Mtor*$^{A/A}$ mice. Primary MEFs were serum starved (20 h), pretreated with the mTOR inhibitor Torin1 (100 nmol/L) (30 min), and stimulated without (−) or with (+) LPS (1 μg/mL) for the times indicated. gr, grams; IB, immunoblot; wk, weeks.

mice (Fig. 2*F*). These primary *Mtor*$^{A/A}$ MEFs displayed impaired LPS stimulated mTORC1/2 signaling (Fig. 2*G*), however, thus confirming inactivation of the TBK1-mTOR axis in response to an innate immune agonist. Consistent with our prior work studying regulation of TBK1-mTOR signaling in response to growth factors (e.g., EGF) in immortalized MEFs (17), LPS but not insulin increased TBK1 P-S172 in primary MEFs (Fig. 2*F* and Supplementary Fig. 2*A*). Curiously, after subjecting the primary MEFs to spontaneous immortalization, insulin-stimulated activation of mTORC1/2 was impaired in immortalized *Mtor*$^{A/A}$ MEFs relative to wild-type MEFs (Supplementary Fig. 2*B* and *C*). As in primary MEFs (Fig. 2*F* and Supplementary Fig. 2*A*), insulin did not increase TBK1 P-S172 in immortalized MEFs (Supplementary Fig. 2*B*). Taken together, these findings suggest that the immortalization process imposes a challenge that renders activation of mTORC1/2 signaling by insulin more dependent on TBK1 action.

Elevated Hyperglycemia, Systemic Insulin Resistance, and Hyperinsulinemia in DIO *Mtor*$^{A/A}$ Mice With No Change in Body Weight

As obesity imposes a pathological challenge that increases systemic insulin resistance and impairs glycemic control (32), we next measured metabolic parameters in DIO *Mtor*$^{+/+}$ and *Mtor*$^{A/A}$ mice. We thus placed male (and female) mice on an HFD starting at 4 weeks of age and studied them longitudinally. Over the course of 20 weeks of HFD feeding, male *Mtor*$^{+/+}$ and *Mtor*$^{A/A}$ mice gained similar amounts of weight (Fig. 3*A*), but ad libitum–fed *Mtor*$^{A/A}$ mice developed hyperglycemia after 8 weeks of HFD feeding (12 weeks old) (Fig. 3*B*). Blood glucose levels were similar after an overnight fast (20 h) (Fig. 3*C*). Beginning at 14 weeks of HFD feeding, DIO *Mtor*$^{A/A}$ mice developed hyperinsulinemia (Fig. 3*D*). At 19 weeks of HFD feeding (23 weeks old), *Mtor*$^{A/A}$ mice displayed significantly elevated systemic insulin resistance compared with wild-type controls (Figs. 3*E* and *F*). Increased insulin resistance in DIO *Mtor*$^{A/A}$ mice is in agreement with their hyperinsulinemia, as it is common for the β-cells of the pancreas to compensate for insulin resistance by secreting more insulin. Glucose tolerance was largely similar in *Mtor*$^{+/+}$ and *Mtor*$^{A/A}$ mice, however (18 weeks of HFD feeding; 22 weeks old) (Fig. 3*G* and *H*), possibly due to elevated plasma insulin levels in fasted *Mtor*$^{A/A}$ mice, an idea consistent with the hyperinsulinemia measured in ad libitum–fed *Mtor*$^{A/A}$ mice (see Fig. 3*D*). The similar body weight of male *Mtor*$^{+/+}$ and *Mtor*$^{A/A}$ mice suggests that the increased insulin resistance of *Mtor*$^{A/A}$ mice results from defects in insulin action and not from differences in energy balance. Insulin resistance in DIO but not lean male mice suggests that obesogenic challenge renders mTOR more dependent on TBK1 action. Curiously, the insulin-resistant phenotype was restricted to male DIO *Mtor*$^{A/A}$ mice, however, as systemic insulin sensitivity was similar in female DIO *Mtor*$^{+/+}$ and *Mtor*$^{A/A}$ mice (Fig. 3*I*). Note that while body weight and fasted (5 h) blood glucose are similar in male DIO *Mtor*$^{+/+}$ and *Mtor*$^{A/A}$ mice, these parameters trended slightly lower in female DIO *Mtor*$^{A/A}$ mice relative to *Mtor*$^{+/+}$ mice (Supplementary Fig. 3*A*–*D*). This observation may explain in part the reduced susceptibility of female *Mtor*$^{A/A}$ mice to obesity-linked insulin resistance.

Unaltered Body Composition but Reduced gWAT Mass and De Novo Lipogenic Gene Expression in DIO *Mtor*$^{A/A}$ Mice

As insulin resistance correlates with the degree of obesity (32), we examined body composition. We found similar overall adiposity and lean mass in male DIO *Mtor*$^{+/+}$ and *Mtor*$^{A/A}$ mice (Fig. 4*A*). gWAT size and mass were reduced in DIO *Mtor*$^{A/A}$ mice (Fig. 4*B* and *C*), however, similar to adipocyte-specific knockout of *Tbk1* or *Raptor* (mTORC1 deficiency) in DIO mice (5,24). H-E staining of gWAT did not reveal gross differences in adipocyte size or adipose tissue organization in DIO *Mtor*$^{A/A}$ mice (Fig. 4*D*). Thus, the increased insulin resistance in DIO *Mtor*$^{A/A}$ mice cannot be explained by increased adiposity. As *Rictor* knockout (mTORC2 deficiency) from adipocytes or hepatocytes was shown to reduce expression of *Chrebp* (a master transcriptional regulator of postprandial de novo lipogenesis [DNL]) and its downstream targets (e.g., *Acl*, *Acc*, *Fasn*) (27,28), we next analyzed expression of these genes in white adipose tissue (WAT) by qPCR. In ad libitum–fed mice, expression of *Acl* was reduced in *Mtor*$^{A/A}$ mice relative to wild-type controls (Fig. 4*E*). Collectively, these findings suggest that TBK1-mTORC2 signaling may contribute to lipogenic gene expression in adipocytes.

Disrupted Insulin-Responsive mTORC1 and mTORC2 Signaling in Metabolic Tissues From DIO *Mtor*$^{A/A}$ Mice

We next examined insulin signaling in vivo in several tissues from DIO *Mtor*$^{+/+}$ and *Mtor*$^{A/A}$ mice. In response to intraperitoneal insulin injection, activation of mTORC1 (S6K1 P-T389) and mTORC2 (Akt P-S473) signaling was impaired in iWAT, gWAT, liver, and skeletal muscle (soleus) from male *Mtor*$^{A/A}$ mice relative to tissues from *Mtor*$^{+/+}$ mice (Fig. 5*A*–*D*). Consistently, results from a study from another group showed that adipocyte-specific knockout of *Tbk1* reduced insulin-stimulated Akt S473 phosphorylation in adipose tissue in DIO mice (5). The insulin signaling deficiency in DIO *Mtor*$^{A/A}$ mice aligns well with their systemic insulin resistance and hyperglycemia. As in MEFs, insulin did not increase TBK1 P-S172 in iWAT or gWAT (Fig. 5*A* and *B*). Consistent with preserved insulin sensitivity (see Fig. 3*I*), insulin-stimulated mTORC1 or mTORC2 signaling remained intact in gWAT from DIO female Mtor$^{A/A}$ mice (Fig. 5*E*).

Reduced Hepatic Lipid Deposition in DIO *Mtor*$^{A/A}$ Mice

As hepatocyte-specific knockout of *Rictor* (mTORC2 deficient) decreases liver mass and lipid deposition while it increases hepatic gluconeogenic gene expression (27), we next measured these parameters in liver tissue from DIO *Mtor*$^{+/+}$ and *Mtor*$^{A/A}$ mice. While liver mass was unchanged (Fig. 6*A*), lipid deposition was reduced in *Mtor*$^{A/A}$ liver, as measured with oil red O staining (Fig. 6*B* and *C*). Consistently, whole-body *Tbk1*$^{\Delta/\Delta}$ mice also showed decreased lipid deposition in the liver (6). Liver tissue from fasted *Mtor*$^{A/A}$ mice displayed trending increases in expression of gluconeogenic genes (i.e., *G6Pase*, *Pepck*, and *Fbp1*) (Fig. 6*D*), which may contribute to elevated hyperglycemia in *Mtor*$^{A/A}$ mice (Fig. 3*B*). Expression of DNL genes (e.g., *Acl*, *Acc*, *Fasn*) also trended lower in liver from ad libitum–fed *Mtor*$^{A/A}$ mice (Supplementary Fig. 4). These data indicate that TBK1-mTOR signaling promotes hepatic lipid deposition and suggest that it may suppress hepatic gluconeogenesis, like mTORC2 function in the liver (6,27).

Increased Proinflammatory and Decreased Anti-inflammatory Gene Expression With Impaired Macrophage M2 Polarization in DIO *Mtor*$^{A/A}$ Mice

During the development of obesity, macrophages infiltrate metabolic tissues and undergo a phenotypic switch from

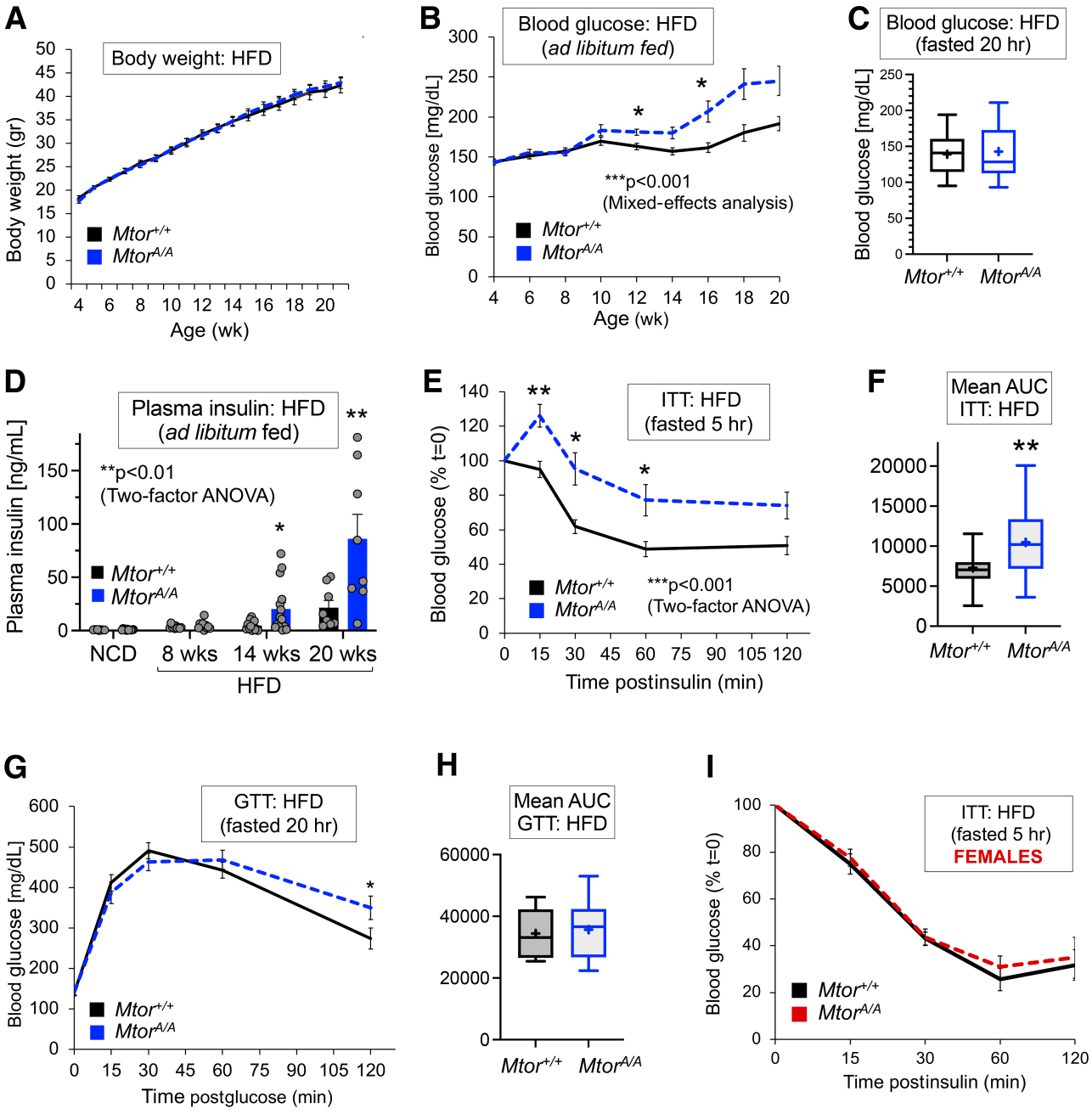

Figure 3—Elevated hyperglycemia, systemic insulin resistance, and hyperinsulinemia in DIO *Mtor*$^{A/A}$ mice with no change in energy balance. *Mtor*$^{+/+}$ and *Mtor*$^{A/A}$ male mice (*A–H*) and female mice (*I*) were fed an HFD for 20 weeks beginning at 4 weeks of age. The following metabolic parameters were measured. *A*: Unaltered body weight in DIO *Mtor*$^{A/A}$ mice. n = 19 *Mtor*$^{+/+}$, 28 *Mtor*$^{A/A}$. *B*: Elevated blood glucose in DIO *Mtor*$^{A/A}$ mice. Biweekly blood glucose in ad libitum–fed mice. n = 19 *Mtor*$^{+/+}$, 28 *Mtor*$^{A/A}$. ***$P < 0.001$ by mixed-effects analysis with multiple comparisons followed by Bonferroni post hoc tests. *C*: Unaltered blood glucose in DIO *Mtor*$^{A/A}$ mice following a 20-h fast. n = 17 *Mtor*$^{+/+}$, 18 *Mtor*$^{A/A}$. *D*: Elevated plasma insulin levels in ad libitum–fed DIO *Mtor*$^{A/A}$ mice. Graph represents mean ± SEM and individual data points. n = 8–13 *Mtor*$^{+/+}$, 8–15 *Mtor*$^{A/A}$. **$P < 0.01$ by two-factor ANOVA with repetition followed by Bonferroni post hoc tests. *E* and *F*: Reduced insulin sensitivity by ITT and area under the curve (AUC) analysis in *Mtor*$^{A/A}$ mice after 19 weeks on HFD. n = 22 *Mtor*$^{+/+}$, 20 *Mtor*$^{A/A}$. For *D*, ***$P < 0.001$ by two-factor ANOVA with repetition followed by Bonferroni post hoc tests. For *F*, **$P < 0.01$ by two-tailed unpaired t test. *G* and *H*: Unaltered glucose tolerance by GTT and area under the curve analysis after 18 weeks on HFD. n = 17 *Mtor*$^{+/+}$, 18 *Mtor*$^{A/A}$. *I*: Unaltered insulin sensitivity in female mice by ITT. n = 7 *Mtor*$^{+/+}$ and *Mtor*$^{A/A}$. Line graphs represent mean ± SEM; box-and-whisker plots represent mean (+), median, and quartiles. Statistical significance: *$P < 0.05$, **$P < 0.01$, ***$P < 0.001$. gr, grams; hr, hours; wk, weeks.

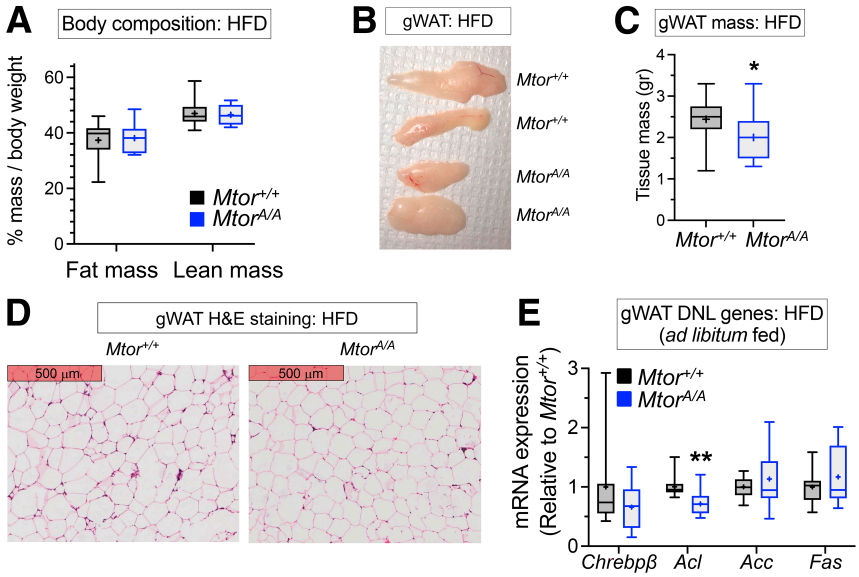

Figure 4—Unaltered body composition but reduced gWAT mass and de novo lipogenic gene expression in DIO *Mtor*$^{A/A}$ mice. *Mtor*$^{+/+}$ and *Mtor*$^{A/A}$ male mice were fed an HFD for 20 weeks. *A*: Body composition by nuclear magnetic resonance at 20 weeks of HFD (24 weeks old). n = 13 *Mtor*$^{+/+}$, 12 *Mtor*$^{A/A}$. *B*: Photos of representative gWAT depots. *C*: gWAT mass. n = 21 *Mtor*$^{+/+}$ and *Mtor*$^{A/A}$. *D*: H-E staining of NBF-fixed, OCT-frozen gWAT sections. Scale bar = 500 μm. *E*: Expression of DNL genes by qRT-PCR. Total RNA was extracted from flash-frozen gWAT obtained from ad libitum–fed mice. n = 12 *Mtor*$^{+/+}$, 13 *Mtor*$^{A/A}$. Box-and-whisker plots represent mean (+), median, and quartiles. *$P < 0.05$ (two-tailed unpaired t test). In panels *A–D*, each lane represents an individual mouse. gr, grams.

alternately activated, more anti-inflammatory M2 states to classically activated, more proinflammatory M1 states (37–39). These events contribute to a state of chronic, low-grade inflammation that correlates with insulin resistance. In mice, myeloid-specific knockout of *Tbk1* increased proinflammatory responses (8), while adipocyte-specific knockout of *Tbk1* or *Raptor* (mTORC1 deficiency), and treatment with rapamycin (an mTORC1-specific inhibitor), increased expression of proinflammatory genes in WAT (5,25,26). We therefore investigated a potential role for TBK1-mTOR signaling in control of these macrophage-related processes. WAT from DIO *Mtor*$^{A/A}$ mice did not show an increase in macrophage infiltration, as mRNA expression and immunohistochemical staining of F4/80, a macrophage marker, were similar in DIO *Mtor*$^{+/+}$ and *Mtor*$^{A/A}$ mice (Figs. 7*A* and *B*). Moreover, mRNA expression of the chemokine genes *Ccl2* (*MCP1*) and *Ccl5* was unchanged (Fig. 7*A*). Expression of some proinflammatory genes (*Cd11c*, *IL-6*) trended upward in WAT from DIO *Mtor*$^{A/A}$ mice (Fig. 7*C*). Consistent with our prior work in which amlexanox or rapamycin reduced IFNβ mRNA and protein levels in response to poly(I:C) in BMDMs (16), expression of IFNβ trended lower in gWAT from DIO *Mtor*$^{A/A}$ mice (Fig. 7*D*). In addition, expression of several anti-inflammatory genes (*Arg1*, *Mgl1* [aka, *Clec10a*], *Mgl2*, *Il-10*, *Fizz1*) trended lower in gWAT from DIO *Mtor*$^{A/A}$ mice (Fig. 7*E*).

BMDMs lacking mTORC2 function due to *Rictor* knockout undergo a phenotypic switch from anti-inflammatory M2 to proinflammatory M1 polarization in a cell-autonomous manner, expressing reduced levels of M2 markers and higher levels of proinflammatory genes (40,41). To evaluate how *Mtor* S2159A knock-in affects macrophage polarization, we isolated BMDMs from *Mtor*$^{+/+}$ and *Mtor*$^{A/A}$ mice and treated them in culture with IL-4 to induce M2 polarization. As expected, IL-4 increased expression of the M2 marker genes *Arg1*, *Mgl1*, *Mgl2*, *Ym1*, and *Fizz1* in wild-type BMDMs (Fig. 7*F–J*). Induction of *Arg1*, *Mgl1*, and *Mgl2* by IL-4 was significantly reduced in *Mtor*$^{A/A}$ BMDMs, with *Ym1* and *Fizz1* expression trending lower. Note that the reduction of these M2 markers in cultured BMDMs from *Mtor*$^{A/A}$ mice mirrors their reduction in gWAT in vivo (Fig. 7*E*). In the absence of IL-4, basal expression of the anti-inflammatory gene *Il-10* was reduced, while basal expression of the proinflammatory genes *Cd11c* and *Tnfα* was increased, in BMDMs from *Mtor*$^{A/A}$ mice, with *Il-6* trending upward (Fig. 7*I* and *K*). Collectively, these findings suggest that TBK1-mTOR signaling promotes macrophage polarization toward M2 and away from M1 states in a cell-autonomous manner.

Elevated TBK1 Activity and mTOR P-S2159 in DIO Mice Relative to Lean Mice

We next sought to understand why reduced TBK1-mTOR signaling increases systemic insulin resistance in the obese but not lean state. We postulated that obesity-associated signals boost TBK1 activity, which phosphorylates mTOR to augment mTORC1/2 signaling. Indeed, we found that WAT depots from wild-type male mice fed an HFD displayed elevated TBK1 P-S172 relative to lean mice fed an NCD (Fig. 8*A*), indicating elevated TBK1 catalytic activity. When mice were administered insulin intraperitoneally, however, insulin did not

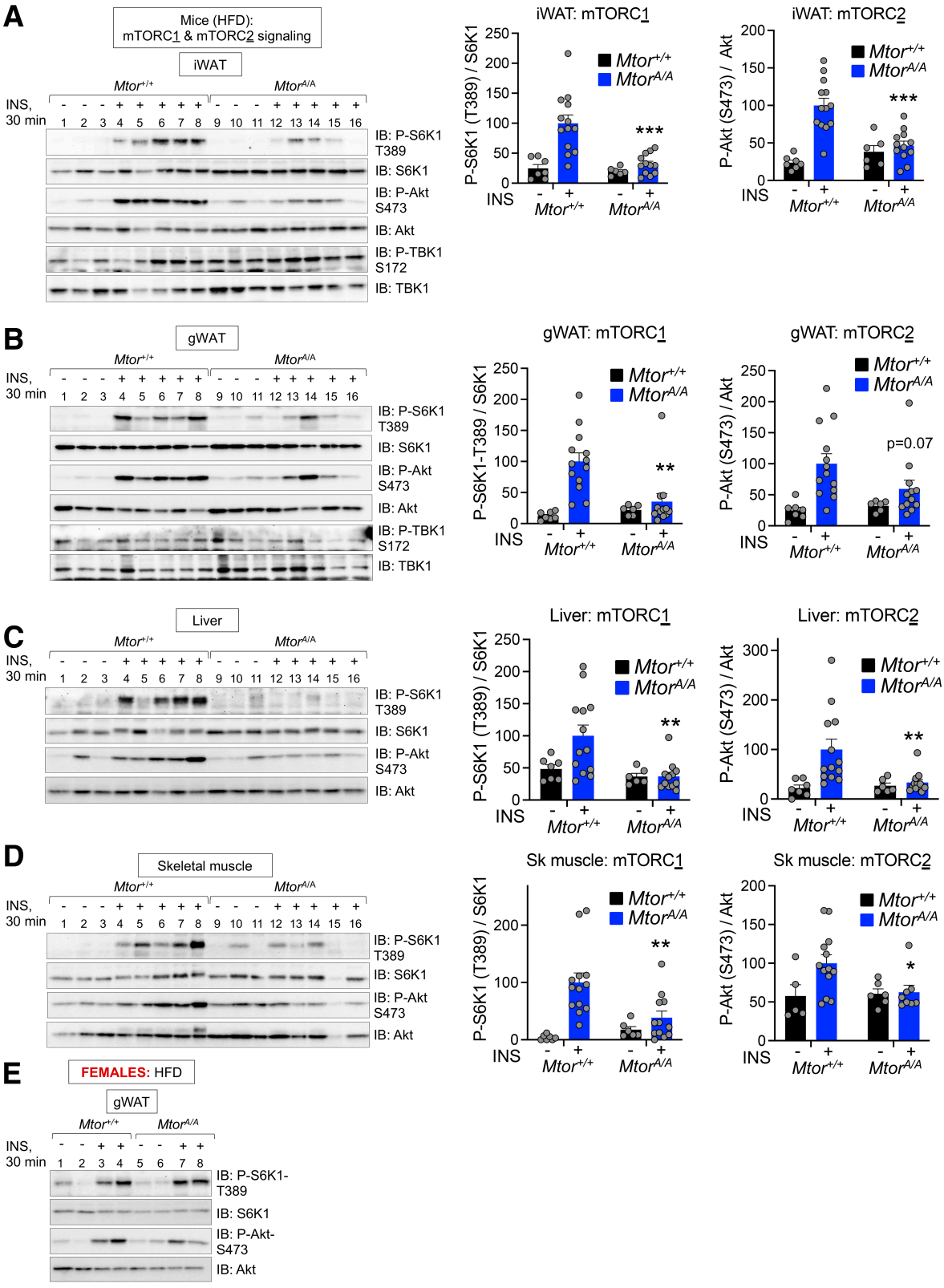

Figure 5—Disrupted insulin responsive mTORC1 and mTORC2 signaling in metabolic tissues from DIO *Mtor*$^{A/A}$ mice. *Mtor*$^{+/+}$ and *Mtor*$^{A/A}$ male mice (*A–D*) or female mice (*E*) were fed an HFD for 20 weeks beginning at 4 weeks of age. Mice were injected without (−) or with (+) insulin (1.3 units/kg body wt i.p., 30 min) following a 5-h fast. Homogenized iWAT (*A*), gWAT (*B* and *E*), liver (*C*), and skeletal (Sk) muscle (*D*) lysates were immunoblotted as indicated. mTORC1 and mTORC2 signaling was quantitated and plotted. Graphs represent mean ± SEM and individual data points from three independent experiments. Total number of male mice per condition per genotype was n = 6–7 (saline) and n = 12–13 (insulin). *$P < 0.05$, **$P < 0.01$, ***$P < 0.001$ relative to DIO *Mtor*$^{+/+}$ mice injected with insulin (two-tailed unpaired t test). IB, immunoblot.

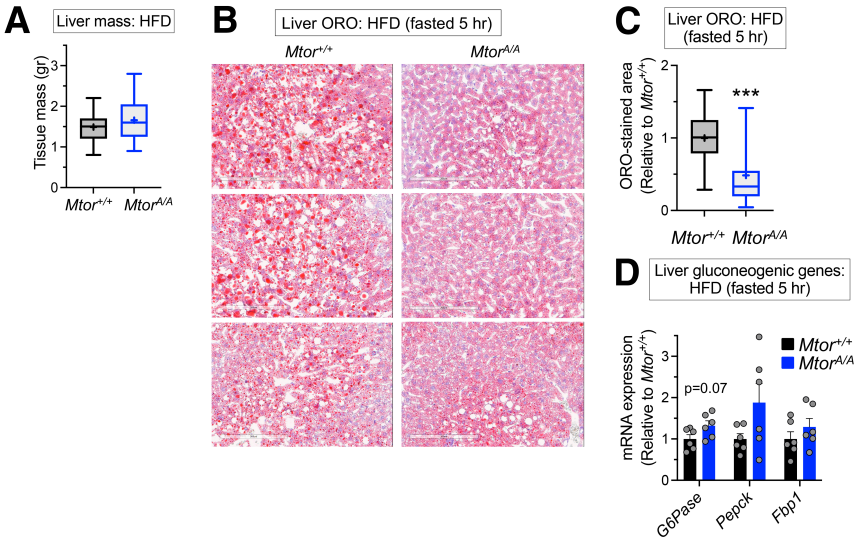

Figure 6—Reduced lipid deposition in liver tissue and elevated gluconeogenic gene expression in DIO $Mtor^{A/A}$ mice. $Mtor^{+/+}$ and $Mtor^{A/A}$ male mice were fed an HFD for 20 weeks. *A*: Liver mass. $n = 21$ $Mtor^{+/+}$ and $Mtor^{A/A}$. *B* and *C*: Oil red O (ORO) staining (*B*) and quantitation (*C*) of NBF-fixed, OCT-frozen liver sections. Quantitation was from $n = 5$ mice per genotype and $n = 10$ images per mouse. $n = 50$ images total per genotype. Scale bar = 200 μm. *D*: Expression of gluconeogenic genes by qRT-PCR. Total RNA was extracted from flash-frozen liver samples obtained from mice that had been fasted for 5.5 h. $n = 6$ $Mtor^{+/+}$ and $Mtor^{A/A}$. Bar graphs represent mean ± SEM and individual data points. Box-and-whisker plots represent mean (+), median, and quartiles. gr, grams; hr, hours.

increase P-TBK1 (Fig. 8*A*), similar to MEFs (Fig. 2*F* and Supplementary Fig. 1*A* and *B*). Consistent with prior work that HFD feeding increases mRNA expression of *IKKε* in WAT and liver (42), we found that HFD feeding increased IKKε protein levels in WAT. Consistent with more modest effects of HFD feeding on *Tbk1* gene expression (5), TBK1 protein levels increased marginally if at all with HFD feeding (Fig. 8*A*). We next asked whether the elevated TBK1 activity in tissue from DIO mice correlates with increased mTOR P-S2159. While we attempted to measure mTOR P-S2159 in mTOR immunoprecipitates from WAT, the signal was too weak to assess reliably. As an alternative approach, we immunoprecipitated mTOR from spleen and liver tissues, finding elevated mTOR P-S2159 in these tissues from DIO mice relative to lean mice (Figs. 8*B* and *C*). As expected, mTOR P-S2159 signal was undetectable in $Mtor^{A/A}$ tissues (Figs. 8*B* and *C*). Taken together, these results support a model whereby obesity-associated signals increase TBK1 activity and mTOR P-S2159, which boost mTORC1/2 signaling (in metabolic cells, macrophages, or both) in parallel to the insulin pathway, thereby attenuating insulin resistance and improving glycemic control during diet-induced obesity (Fig. 8*D*).

DISCUSSION

With the rising incidence of obesity worldwide it is important to better define the mechanisms underlying obesity-linked metabolic comorbidities including insulin resistance, chronic inflammation, and type 2 diabetes (32,38,43,44). By studying DIO $Mtor^{A/A}$ mice, we demonstrate that TBK1-mTOR signaling attenuates insulin resistance to improve glycemic control in DIO mice. These findings suggest that boosting TBK1-mTOR signaling may ameliorate insulin resistance in people with obesity, presenting a potential opportunity for therapeutic intervention. We speculate further that a reduced level of TBK1-responsive mTOR signaling in a subset of obese individuals may render them more prone to development of type 2 diabetes than others.

Our prior work in intact cells supports the idea that TBK1 represents a major mTOR S2159 kinase (16,17). We cannot exclude the possibility, however, that IKKε or other kinase(s) phosphorylates mTOR S2159 to control glucose metabolism in vivo. It also remains possible that TBK1 phosphorylates other sites on mTOR (or on mTOR partner proteins). As adipocyte-specific knockout of *Tbk1* reduced insulin-stimulated Akt S473 phosphorylation in WAT in vivo (5), this finding supports the idea that TBK1 promotes mTOR signaling as part of mTORC2 in vivo. While our global *Mtor* S2159A knock-in model cannot assign definitively specific metabolic roles for TBK1 signaling to mTORC1 versus mTORC2, it offers a distinct advantage: it reduces rather than ablates mTOR function by removing a distinct regulatory input. This precise molecular manipulation decreases the possibility that compensatory rewiring alters phenotypes, a potential pitfall of chronic knockout models. In addition, the mTOR S2159A mutation removes a distinct TBK1 effector function (regulation of mTOR) rather than all TBK1 functions. Thus, our model manipulates TBK1 and mTOR signaling in a more subtle and likely more physiologically relevant way.

Based on shared phenotypes between *Mtor* S2159A knock-in mice and those with tissue-specific knockout of *Tbk1*, *Mtor*, *Raptor*, or *Rictor* (5,24,25,27,28,33), we propose that

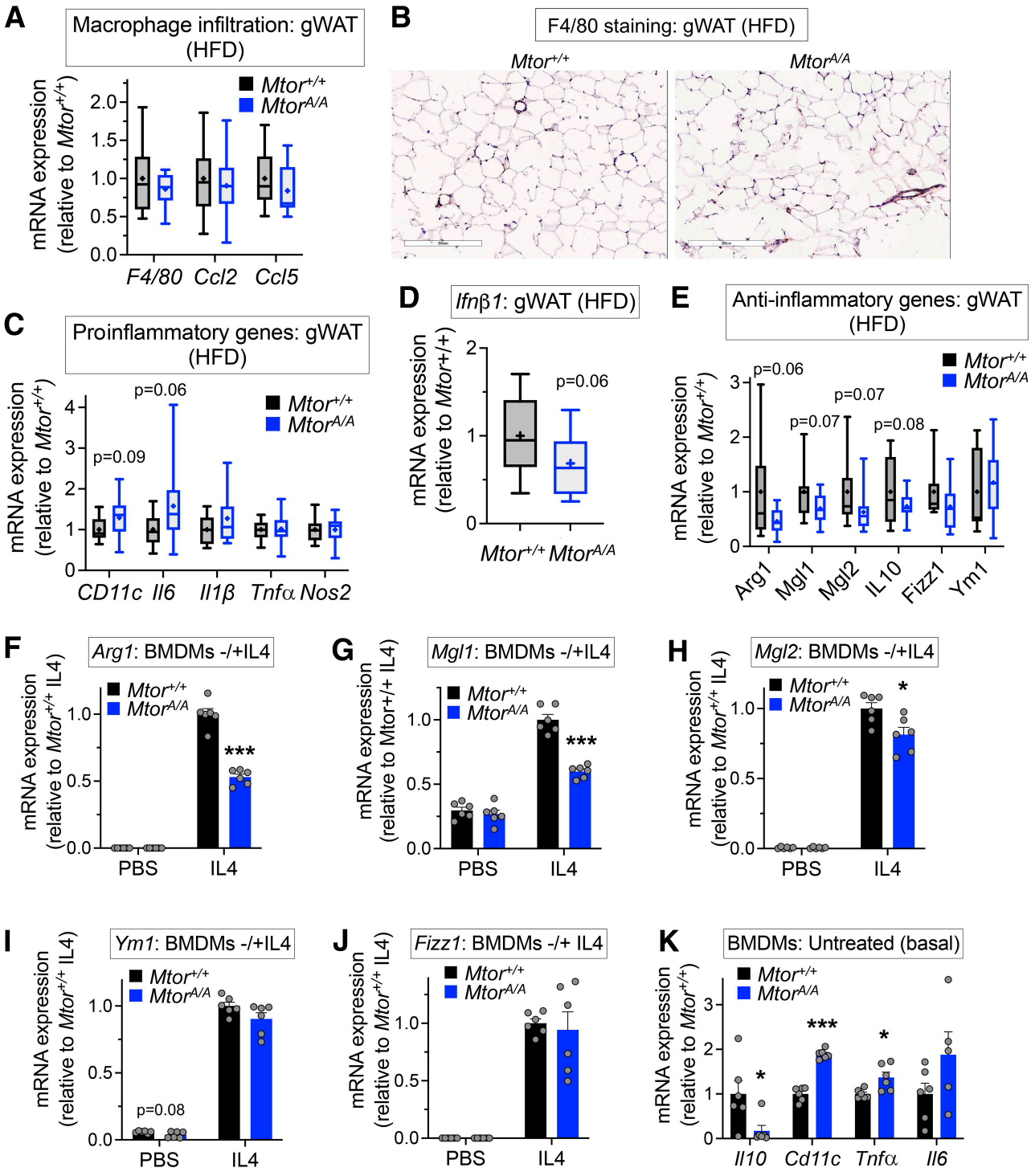

Figure 7—Increased proinflammatory and decreased anti-inflammatory gene expression and impaired macrophage M2 polarization in DIO *Mtor*$^{A/A}$ mice. *Mtor*$^{+/+}$ and *Mtor*$^{A/A}$ male mice were fed an HFD for 20 weeks. *A* and *C–E*: Total RNA was extracted from flash-frozen gWAT for qRT-PCR analysis of the indicated immunomodulatory genes. n = 12 *Mtor*$^{+/+}$, 13 *Mtor*$^{A/A}$. *B*: F4/80 staining of NBF-fixed, OCT-frozen gWAT. Scale bar = 300 μm. *F–J*: Primary BMDMs from lean male *Mtor*$^{+/+}$ and *Mtor*$^{A/A}$ mice (8–14 weeks old) were untreated (−) (PBS) or treated with IL-4 (+) (10 ng/mL, 24 h). Total RNA was extracted for qRT-PCR analysis of cytokine and macrophage marker genes. Relative mRNA expression was calculated from two independent experiments performed in triplicate using the ΔΔCT method. *K*: As in *F–J*, except basal levels of mRNA were measured in cells treated with PBS only. Box-and-whisker plots represent mean (+), median, and quartiles. Bar graphs represent mean ± SEM and individual data points. *$P < 0.05$; ***$P < 0.001$ (two-tailed unpaired *t* test).

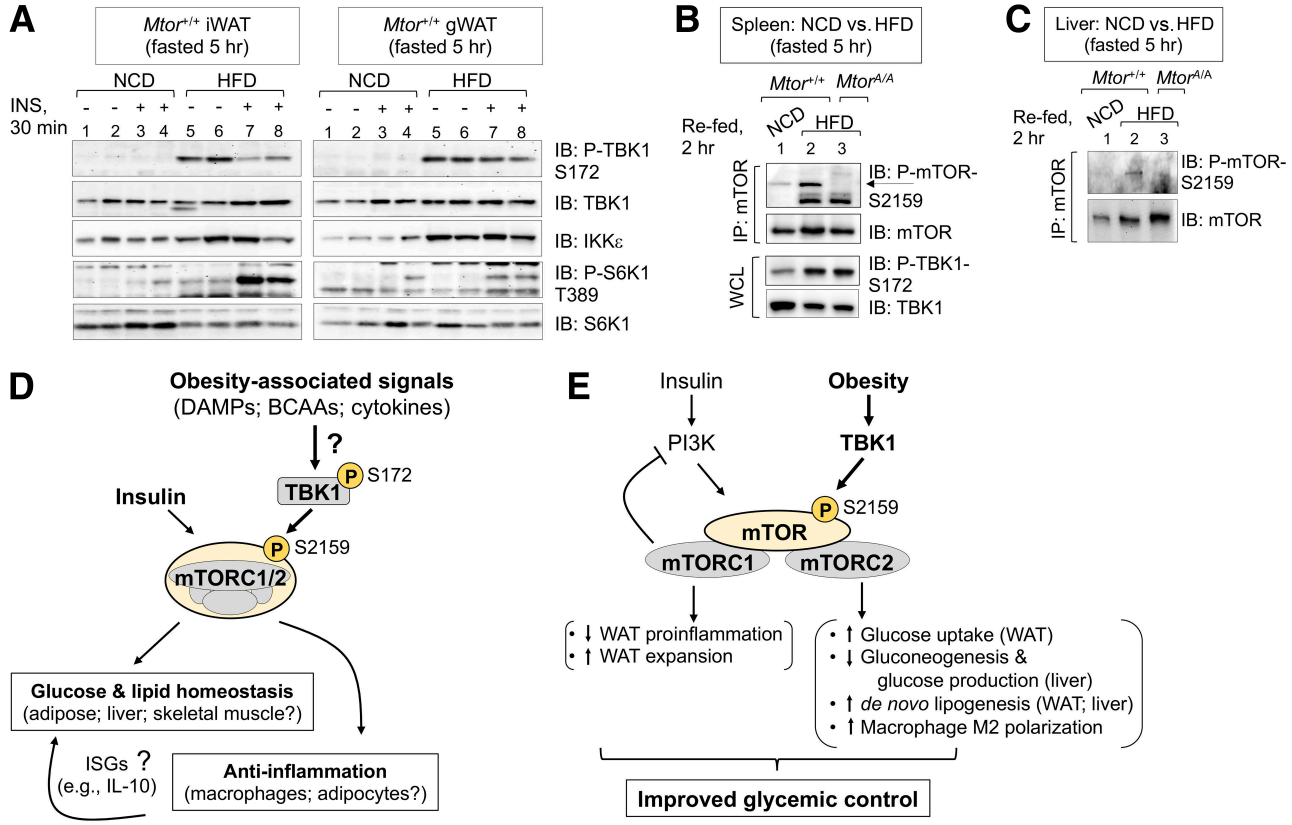

Figure 8—Elevated TBK1 activity and mTOR P-S2159 in DIO mice relative to lean mice. *A*: *Mtor*$^{+/+}$ male mice were fed an NCD (8–14 weeks old) or an HFD for 20 weeks beginning at 4 weeks old (24 weeks old). Animals were then injected intraperitoneally without (-) or with (+) 1.0 units/kg body wt insulin (NCD) or 1.3 units/kg body wt insulin (HFD) (30 min) following a 5-h fast. iWAT and gWAT were harvested, lysed, and immunoblotted as indicated. Each lane represents an individual mouse. *B* and *C*: *Mtor*$^{+/+}$ male mice were fed an NCD (8–14 weeks old), and both *Mtor*$^{+/+}$ and *Mtor*$^{A/A}$ male mice were fed an HFD for 20 weeks beginning at 4 weeks old (24 weeks old). Animals were refed for 2 h following a 5-h fast. mTOR was immunoprecipitated (IP) from spleen and liver lysates, and immunoprecipitated mTOR and whole cell lysates (WCL) were immunoblotted as indicated. Each lane represents an individual mouse. *D*: Model, obesity-associated signals increase TBK1 activity and mTOR P-S2159, which boosts mTORC1 and mTORC2 signaling to improve glycemic control in the obese but not lean state. *E*: Model, potential mechanisms for glycemic control by TBK1-mTORC1 and TBK1-mTORC2 signaling in diet-induced obesity. BCAAs, branched-chain amino acids; DAMPS, damage-associated molecular patterns; hr, hours; IB, immunoblot; ISGs, interferon-stimulated genes.

TBK1 signals through both mTORC1 and mTORC2 in adipocytes and hepatocytes to protect against obesity-linked metabolic disease (Fig. 8*E*). Considering the published literature, we propose more specifically that TBK1-mTORC1 signaling in adipocytes may promote adipocyte differentiation and the healthy expansion of WAT as obesity progresses (15,24,45), while it may attenuate adipose tissue inflammation (5,7,25) (Fig. 8*E*). TBK1-mTORC2 signaling in adipocytes may promote de novo lipogenic gene expression and glucose uptake in response to insulin (28,46). TBK1-mTORC2 signaling in hepatocytes may suppress hepatic gluconeogenic gene expression and glucose production and may promote lipid storage (27). Note that in contrast to *Mtor*$^{A/A}$ and *Tbk1*$^{\Delta/\Delta}$ mice (6), however, hepatocyte-specific *Tbk1* knockout increased triglyceride deposition in the liver (47). As *Mtor* S2159A reduces insulin-stimulated mTORC1 and mTORC2 signaling in skeletal muscle, this tissue may also represent an important site for glycemic control by TBK1-mTOR.

Nutrient overload during obesity hyperactivates mTORC1 and S6K1, which contributes to insulin resistance by mediating negative feedback on PI3K flux through inhibitory IRS-1 phosphorylation, thus attenuating insulin-PI3K signaling to mTORC2, Akt, and other PI3K-responsive targets (48–53) (Fig. 8*E*). Thus, decreased mTORC1 signaling during obesity is predicted to improve insulin sensitivity. Indeed, adipocyte-specific knockout of S6K1, an mTORC1 target, improved insulin sensitivity in DIO mice (although this effect may result largely or in part from resistance to diet-induced obesity) (48); in addition, pharmacological inhibition of S6K1 improved insulin sensitivity in DIO mice (52). Reduced TBK1-mTOR signaling in our *Mtor*$^{A/A}$ mice would thus be expected to increase systemic insulin sensitivity. Yet, we found the opposite phenotype increased, not decreased, insulin resistance in DIO *Mtor*$^{A/A}$ mice. The solution to this apparent paradox lies in the ability of TBK1 to boost mTORC2 signaling in parallel to the insulin/PI3K pathway (Fig. 8*E*). While reduced TBK1-mTORC1 signaling might increase insulin sensitivity in our *Mtor*$^{A/A}$ mice, a

concomitant reduction in TBK1-mTORC2 signaling likely negates this benefit. Reduced TBK1-mTORC1 signaling, however, also reduces gWAT mass and anti-inflammatory gene expression in adipose tissue and macrophages, which may contribute to the net effect of exacerbated insulin resistance. It is important to note that chronic treatment of mice with rapamycin, an allosteric inhibitor that acutely inhibits mTORC1, increases insulin resistance—rather than reducing it—by suppressing mTORC2 assembly and activity (54,55). Thus, *Mtor* S2159A knock-in phenocopies chronic rapamycin-induced insulin resistance.

Whether TBK1-mTOR signaling in macrophages improves glycemic control during diet-induced obesity remains an important unresolved question. Recent work demonstrated that myeloid-specific knockout of *Tbk1* (using the LysM-Cre driver) exacerbates systemic insulin resistance and inflammation of adipose tissue in DIO mice (8), like our $Mtor^{A/A}$ mice. In addition, activation of PI3K in macrophages by TLR engagement, which activates both mTORC1 and mTORC2, restricts proinflammatory responses (41,56). Moreover, reduced mTORC2 function in myeloid cells shifts macrophage polarization away from an anti-inflammatory M2 state and toward a proinflammatory M1 state, like *Mtor* S2159A knock-in (40,41). Together, these findings support the idea that TBK1-mTOR signaling in macrophages promotes anti-inflammatory responses, which may improve insulin sensitivity during diet-induced obesity. In contrast, however, knockout of *Raptor* in myeloid cells decreased systemic insulin resistance and adipose tissue inflammation, while myeloid-specific knockout of *Rictor* had no effect on these parameters (41,57). Additional work will be required to determine whether a more subtle alteration of mTOR function in macrophages (i.e., elimination of the upstream TBK1 input) affects insulin sensitivity and inflammatory state during obesity.

Results of a recent study demonstrated that in response to postprandial signals, adipose tissue macrophages secrete IL-10, which circulates and cooperates with insulin to suppress hepatic gluconeogenic gene expression and glucose production, the disruption of which impairs glycemic control in DIO mice (58). In addition, treatment of BMDMs in culture with insulin and LPS increased expression of IL-10 in a PI3K/TSC/Akt-dependent manner (i.e., thus, via mTORC1), and IL-10 cooperated with insulin in primary hepatocytes in culture to suppress gluconeogenic gene expression and glucose production (58). As *Mtor* S2159A knock-in reduces expression of *Ifnβ* and its target *Il-10* in WAT of DIO mice, we suggest that TBK1-mTOR signaling in macrophages may improve glycemic control during obesity by promoting expression and secretion of interferon-stimulated gene products (e.g., IL-10) that attenuate inflammation and sensitize target tissues to insulin action (Fig. 8*D*).

What explains the insulin-sensitizing effect of TBK1-mTOR signaling in obese but not lean male mice? We speculate that obesity-associated signals increase TBK1 activity and mTOR S2159 phosphorylation in parallel to the insulin/PI3K pathway (Fig. 8*D* and *E*), as insulin failed to increase TBK1 S172 phosphorylation in gWAT in vivo or MEFs in culture. Such signals could derive from elevated levels of damage-associated molecular patterns (e.g., RNA from dead adipocytes, gut-derived LPS, saturated fatty acids) (59–61) that activate TLR signaling, branched-chain amino acids, or proinflammatory cytokines, all of which rise with obesity (62). Indeed, we found elevated TBK1 (S172) and mTOR (S2159) phosphorylation in tissues from wild-type DIO mice relative to lean mice. This observation agrees with those of Reilly et al. (3) and Cruz et al. (6), who found upregulated phosphorylation of TBK1 (S172) and its target IRF3 (S396), as well as upregulated TBK1 catalytic activity, in WAT from DIO mice relative to lean mice. What explains the sex-specific effect of *Mtor* S2159A knock-in on mTORC1/2 signaling and systemic insulin sensitivity during diet-induced obesity? While we do not know currently, we speculate that female DIO $Mtor^{A/A}$ mice fail to display increased insulin resistance and hyperglycemia, unlike male DIO $Mtor^{A/A}$ mice, due to beneficial effects of female sex hormones on adipose tissue biology and metabolism (63). In future work, it will be interesting to determine whether female $Mtor^{A/A}$ mice respond to HFD and induction of obesity by upregulating mTOR P-S2159.

In conclusion, the findings of this study identify TBK1 as an activator of mTOR in vivo and reveal that TBK1-mTOR signaling mediates homeostatic responses that counter obesity-linked insulin resistance. Importantly, we demonstrate that site-specific mTOR phosphorylation controls mammalian metabolism in vivo. Future work is needed to address important unresolved questions including which obesity-associated signals activate TBK1 posttranslationally and whether TBK1-mTOR signaling in metabolic cells (e.g., adipocytes, hepatocytes, skeletal myocytes), macrophages, or both mediates protective metabolic effects during diet-induced obesity. Whether IKKε contributes to mTOR-mediated metabolic control in vivo also remains unclear. Clinically, our findings suggest that boosting TBK1-mTOR signaling in people with obesity may represent a beneficial therapeutic strategy to improve glycemic control. Further molecular dissection of TBK1 and mTOR signaling will be required for an understanding of how these multifunctional kinases control diverse physiological processes related to metabolism, innate immunity, and tumorigenesis and whether they do so together through the TBK1-mTOR pathway.

Acknowledgments. The authors thank Ormond MacDougald (University of Michigan Medical School) for assistance with isolation of adipose tissue depots from mice, Ben Allen (University of Michigan Medical School) for assistance with isolation of MEFs, and Daniel Lucas (University of Cincinnati) for assistance with isolation of primary BMDMs.

Funding. This work was supported by National Institute of Diabetes and Digestive and Kidney Diseases, National Institutes of Health (NIH), grants R01-DK103877 and R56-DK126328 to D.C.F. and by the Michigan Diabetes Research Center (NIH grant P30-DK020572).

Duality of Interest. No potential conflicts of interest relevant to this article were reported.

Author Contributions. T.M.B., M.G.M., and D.C.F. designed the *Mtor*$^{A/A}$ mouse model (the UM Molecular Genetics and Transgenics Core generated the *Mtor*$^{A/A}$ mouse model). C.B., D.K., K.H., and K.W.C. performed experiments. C.B., M.G.M., and D.C.F. designed experiments. C.B. and D.C.F. analyzed data and interpreted the results. C.N.L. consulted on certain experiments. C.B. wrote the manuscript, and D.C.F. edited the manuscript. D.C.F. is the guarantor of this work and, as such, had full access to all the data in the study and takes responsibility for the integrity of the data and the accuracy of the data analysis.

References

1. Mogensen TH. Pathogen recognition and inflammatory signaling in innate immune defenses. Clin Microbiol Rev 2009;22:240–273
2. Yu T, Yi YS, Yang Y, Oh J, Jeong D, Cho JY. The pivotal role of TBK1 in inflammatory responses mediated by macrophages. Mediators Inflamm 2012; 2012:979105
3. Reilly SM, Chiang SH, Decker SJ, et al. An inhibitor of the protein kinases TBK1 and IKK-ε improves obesity-related metabolic dysfunctions in mice. Nat Med 2013;19:313–321
4. Oral EA, Reilly SM, Gomez AV, et al. Inhibition of IKKε and TBK1 improves glucose control in a subset of patients with type 2 diabetes. Cell Metab 2017;26:157–170.e7
5. Zhao P, Wong KI, Sun X, et al. TBK1 at the crossroads of inflammation and energy homeostasis in adipose tissue. Cell 2018;172:731–743.e12
6. Cruz VH, Arner EN, Wynne KW, Scherer PE, Brekken RA. Loss of Tbk1 kinase activity protects mice from diet-induced metabolic dysfunction. Mol Metab 2018;16:139–149
7. Zhao P, Saltiel AR. Interaction of adipocyte metabolic and immune functions through TBK1. Front Immunol 2020;11:592949
8. Gao T, Liu T, Ko CJ, et al. Myeloid cell TBK1 restricts inflammatory responses. Proc Natl Acad Sci U S A 2022;119:e2107742119
9. Durand JK, Zhang Q, Baldwin AS. Roles for the IKK-related kinases TBK1 and IKKε in cancer. Cells 2018;7:139
10. Revach OY, Liu S, Jenkins RW. Targeting TANK-binding kinase 1 (TBK1) in cancer. Expert Opin Ther Targets 2020;24:1065–1078
11. Valvezan AJ, Manning BD. Molecular logic of mTORC1 signalling as a metabolic rheostat. Nat Metab 2019;1:321–333
12. Kim J, Guan KL. mTOR as a central hub of nutrient signalling and cell growth. Nat Cell Biol 2019;21:63–71
13. Liu, GY, Sabatini, DM. mTOR at the nexus of nutrition, growth, ageing and disease. Nat Rev Mol Cell Biol 2020;21:183–203
14. Szwed A, Kim E, Jacinto E. Regulation and metabolic functions of mTORC1 and mTORC2. Physiol Rev 2021;101:1371–1426
15. Lee PL, Jung SM, Guertin DA. The complex roles of mechanistic target of rapamycin in adipocytes and beyond. Trends Endocrinol Metab 2017;28: 319–339
16. Bodur C, Kazyken D, Huang K, et al. The IKK-related kinase TBK1 activates mTORC1 directly in response to growth factors and innate immune agonists. EMBO J 2018;37:19–38
17. Tooley AS, Kazyken D, Bodur C, Gonzalez IE, Fingar DC. The innate immune kinase TBK1 directly increases mTORC2 activity and downstream signaling to Akt. J Biol Chem 2021;297:100942
18. Cooper JM, Ou YH, McMillan EA, et al. TBK1 provides context-selective support of the activated AKT/mTOR pathway in lung cancer. Cancer Res 2017;77:5077–5094
19. Zhu L, Li Y, Xie X, et al. TBKBP1 and TBK1 form a growth factor signalling axis mediating immunosuppression and tumourigenesis. Nat Cell Biol 2019;21:1604–1614
20. Hoxhaj G, Manning BD. The PI3K-AKT network at the interface of oncogenic signalling and cancer metabolism. Nat Rev Cancer 2020;20:74–88
21. Fu W, Hall MN. Regulation of mTORC2 Signaling. Genes (Basel) 2020; 11:1045
22. Sarbassov DD, Guertin DA, Ali SM, Sabatini DM. Phosphorylation and regulation of Akt/PKB by the rictor-mTOR complex. Science 2005;307:1098–1101
23. Kazyken D, Magnuson B, Bodur C, et al. AMPK directly activates mTORC2 to promote cell survival during acute energetic stress. Sci Signal 2019;12:eaav3249
24. Lee PL, Tang Y, Li H, Guertin DA. Raptor/mTORC1 loss in adipocytes causes progressive lipodystrophy and fatty liver disease. Mol Metab 2016;5:422–432
25. Chimin P, Andrade ML, Belchior T, et al. Adipocyte mTORC1 deficiency promotes adipose tissue inflammation and NLRP3 inflammasome activation via oxidative stress and de novo ceramide synthesis. J Lipid Res 2017;58:1797–1807
26. Paschoal VA, Amano MT, Belchior T, et al. mTORC1 inhibition with rapamycin exacerbates adipose tissue inflammation in obese mice and dissociates macrophage phenotype from function. Immunobiology 2017;222:261–271
27. Hagiwara A, Cornu M, Cybulski N, et al. Hepatic mTORC2 activates glycolysis and lipogenesis through Akt, glucokinase, and SREBP1c. Cell Metab 2012;15:725–738
28. Tang Y, Wallace M, Sanchez-Gurmaches J, et al. Adipose tissue mTORC2 regulates ChREBP-driven de novo lipogenesis and hepatic glucose metabolism. Nat Commun 2016;7:11365
29. Clark K, Plater L, Peggie M, Cohen P. Use of the pharmacological inhibitor BX795 to study the regulation and physiological roles of TBK1 and IkappaB kinase epsilon: a distinct upstream kinase mediates Ser-172 phosphorylation and activation. J Biol Chem 2009;284:14136–14146
30. Ma X, Helgason E, Phung QT, et al. Molecular basis of Tank-binding kinase 1 activation by transautophosphorylation. Proc Natl Acad Sci USA 2012;109:9378–9383
31. Ivashkiv LB, Donlin LT. Regulation of type I interferon responses. Nat Rev Immunol 2014;14:36–49
32. Czech MP. Insulin action and resistance in obesity and type 2 diabetes. Nat Med 2017;23:804–814
33. Shan T, Zhang P, Jiang Q, Xiong Y, Wang Y, Kuang S. Adipocyte-specific deletion of mTOR inhibits adipose tissue development and causes insulin resistance in mice. Diabetologia 2016;59:1995–2004
34. Acosta-Jaquez HA, Keller JA, Foster KG, et al. Site-specific mTOR phosphorylation promotes mTORC1-mediated signaling and cell growth. Mol Cell Biol 2009;29:4308–4324
35. Todaro GJ, Green H. Quantitative studies of the growth of mouse embryo cells in culture and their development into established lines. J Cell Biol 1963;17:299–313
36. Xu, J. Preparation, culture, and immortalization of mouse embryonic fibroblasts. Curr Protoc Mol Biol 2005;Chapter 28:Unit 28.1
37. Russo L, Lumeng CN. Properties and functions of adipose tissue macrophages in obesity. Immunology 2018;155:407–417
38. Lee YS, Wollam J, Olefsky JM. An integrated view of immunometabolism. Cell 2018;172:22–40
39. Appari M, Channon KM, McNeill E. Metabolic regulation of adipose tissue macrophage function in obesity and diabetes. Antioxid Redox Signal 2018;29: 297–312
40. Byles V, Covarrubias AJ, Ben-Sahra I, et al. The TSC-mTOR pathway regulates macrophage polarization. Nat Commun 2013;4:2834
41. Festuccia WT, Pouliot P, Bakan I, Sabatini DM, Laplante M. Myeloid-specific Rictor deletion induces M1 macrophage polarization and potentiates in vivo pro-inflammatory response to lipopolysaccharide. PLoS One 2014;9:e95432
42. Chiang SH, Bazuine M, Lumeng CN, et al. The protein kinase IKKepsilon regulates energy balance in obese mice. Cell 2009;138:961–975
43. Ye J, McGuinness OP. Inflammation during obesity is not all bad: evidence from animal and human studies. Am J Physiol Endocrinol Metab 2013;304:E466–E477
44. Reilly SM, Saltiel AR. Adapting to obesity with adipose tissue inflammation. Nat Rev Endocrinol 2017;13:633–643
45. Carnevalli LS, Masuda K, Frigerio F, et al. S6K1 plays a critical role in early adipocyte differentiation. Dev Cell 2010;18:763–774

46. Uhm M, Bazuine M, Zhao P, et al. Phosphorylation of the exocyst protein Exo84 by TBK1 promotes insulin-stimulated GLUT4 trafficking. Sci Signal 2017;10:eaah5085
47. Huh JY, Reilly SM, Abu-Odeh M, et al. TANK-binding kinase 1 regulates the localization of acyl-CoA synthetase ACSL1 to control hepatic fatty acid oxidation. Cell Metab 2020;32:1012–1027.e7
48. Um SH, Frigerio F, Watanabe M, et al. Absence of S6K1 protects against age- and diet-induced obesity while enhancing insulin sensitivity. Nature 2004;431:200–205
49. Um SH, D'Alessio D, Thomas G. Nutrient overload, insulin resistance, and ribosomal protein S6 kinase 1, S6K1. Cell Metab 2006;3:393–402
50. Harrington LS, Findlay GM, Lamb RF. Restraining PI3K: mTOR signalling goes back to the membrane. Trends Biochem Sci 2005;30:35–42
51. Catalán V, Gómez-Ambrosi J, Rodríguez A, et al. Expression of S6K1 in human visceral adipose tissue is upregulated in obesity and related to insulin resistance and inflammation. Acta Diabetol 2015;52:257–266
52. Shum M, Bellmann K, St-Pierre P, Marette A. Pharmacological inhibition of S6K1 increases glucose metabolism and Akt signalling in vitro and in diet-induced obese mice. Diabetologia 2016;59:592–603
53. Binsch C, Jelenik T, Pfitzer A, et al. Absence of the kinase S6k1 mimics the effect of chronic endurance exercise on glucose tolerance and muscle oxidative stress. Mol Metab 2017;6:1443–1453
54. Lamming DW, Ye L, Katajisto P, et al. Rapamycin-induced insulin resistance is mediated by mTORC2 loss and uncoupled from longevity. Science 2012;335:1638–1643
55. Sarbassov DD, Ali SM, Sengupta S, et al. Prolonged rapamycin treatment inhibits mTORC2 assembly and Akt/PKB. Mol Cell 2006;22:159–168
56. Troutman TD, Bazan JF, Pasare C. Toll-like receptors, signaling adapters and regulation of the pro-inflammatory response by PI3K. Cell Cycle 2012;11:3559–3567
57. Jiang H, Westerterp M, Wang C, Zhu Y, Ai D. Macrophage mTORC1 disruption reduces inflammation and insulin resistance in obese mice. Diabetologia 2014;57:2393–2404
58. Toda G, Soeda K, Okazaki Y, et al. Insulin- and lipopolysaccharide-mediated signaling in adipose tissue macrophages regulates postprandial glycemia through Akt-mTOR activation. Mol Cell 2020;79:43–53.e4
59. Karikó K, Ni H, Capodici J, Lamphier M, Weissman D. mRNA is an endogenous ligand for Toll-like receptor 3. J Biol Chem 2004;279:12542–12550
60. Suganami T, Tanimoto-Koyama K, Nishida J, et al. Role of the Toll-like receptor 4/NF-kappaB pathway in saturated fatty acid-induced inflammatory changes in the interaction between adipocytes and macrophages. Arterioscler Thromb Vasc Biol 2007;27:84–91
61. Cani PD, Bibiloni R, Knauf C, et al. Changes in gut microbiota control metabolic endotoxemia-induced inflammation in high-fat diet-induced obesity and diabetes in mice. Diabetes 2008;57:1470–1481
62. White PJ, McGarrah RW, Herman MA, Bain JR, Shah SH, Newgard CB. Insulin action, type 2 diabetes, and branched-chain amino acids: A two-way street. Mol Metab 2021;52:101261
63. Palmer BF, Clegg DJ. The sexual dimorphism of obesity. Mol Cell Endocrinol 2015;402:113–119